Biogeosciences Discuss., 8, 11863–11897, 2011
www.biogeosciences-discuss.net/8/11863/2011/
doi:10.5194/bgd-8-11863-2011

Biogeosciences Discussions

Calcium carbonate production response to future ocean warming and acidification

A. J. Pinsonneault[1,2], H. D. Matthews[1], E. D. Galbraith[3], and A. Schmittner[4]

[1]Department of Geography, Planning and Environment, Concordia University, 1455 de Maisonneuve Blvd W., Montreal, QC, H3G 1M8, Canada
[2]Department of Geography, McGill University, 805 Sherbrooke Street West, Montreal, QC, H3A 2K6, Canada
[3]Department of Earth and Planetary Sciences, McGill University, 3450 University, Montreal, QC, H3A 2A7, Canada,
[4]College of Oceanic and Atmospheric Sciences, Oregon State University, 104 COAS Administration Building, Corvallis OR 97331–5503, USA

Received: 16 November 2011 – Accepted: 1 December 2011 – Published: 13 December 2011

Correspondence to: A. J. Pinsonneault (andrew.pinsonneault@mail.mcgill.ca)

Published by Copernicus Publications on behalf of the European Geosciences Union.

Abstract

Anthropogenic carbon dioxide (CO_2) emissions are acidifying the ocean, affecting calcification rates in pelagic organisms and thereby modifying the oceanic alkalinity cycle. However, the responses of pelagic calcifying organisms to acidification vary widely between species, contributing uncertainty to predictions of atmospheric CO_2 and the resulting climate change. Meanwhile, ocean warming caused by rising CO_2 is expected to drive increased growth rates of all pelagic organisms, including calcifiers. It thus remains unclear whether anthropogenic CO_2 will ultimately increase or decrease the globally-integrated pelagic calcification rate. Here, we assess the importance of this uncertainty by introducing a variable dependence of calcium carbonate ($CaCO_3$) production on calcite saturation state (Ω_{CaCO_3}) in the University of Victoria Earth System Climate Model, an intermediate complexity coupled carbon-climate model. In a series of model simulations, we examine the impact of this parameterization on global ocean carbon cycling under two CO_2 emissions scenarios, both integrated to the year 3500. The simulations show a significant sensitivity of the vertical and surface horizontal alkalinity gradients to the parameterization, as well as the removal of alkalinity from the ocean through $CaCO_3$ burial. These sensitivities result in an additional oceanic uptake of carbon when calcification depends on Ω_{CaCO_3} (of up to 13 % of total carbon emissions), compared to the case where calcification is insensitive to acidification. In turn, this response causes a reduction of global surface air temperature of up to 0.4 °C in year 3500, a 13 % reduction in the amplitude of warming. Narrowing these uncertainties will require better understanding of both temperature and acidification effects on pelagic calcifiers. Preliminary examination suggests that alkalinity observations can be used to constrain the range of uncertainties and may exclude large sensitivities of $CaCO_3$ production on Ω_{CaCO_3}.

BGD
8, 11863–11897, 2011

1 Introduction

Ocean uptake of atmospheric carbon dioxide (CO_2) is having a profound effect on biochemical cycles and ocean ecosystems. Increased CO_2 dissolution in the surface ocean leads to a decrease in seawater pH (Secretariat of the Convention on Biological Diversity, 2009, hereafter SCBD, 2009). This, in turn, leads to a decrease in carbonate ion concentration ($[CO_3^{2-}]$), a shoaling of the calcium carbonate ($CaCO_3$) saturation horizon and lysocline, and an alteration of $CaCO_3$ stored in deep-sea sediments. This process, known as ocean acidification, has the potential to severely impact the biological carbon pumps, which influence the vertical alkalinity and dissolved inorganic carbon (DIC) gradients in the ocean. This, in turn, would affect the strength of the ocean as a carbon sink and, ultimately, the rate and magnitude of global climate change.

Biogenic calcification describes the formation of $CaCO_3$ by certain species of marine biota that use $CaCO_3$ to create their shells and skeletons (Doney et al., 2009; SCBD, 2009). In general, the rate of biogenic calcification depends on the saturation state of $CaCO_3$ in the surface ocean defined as:

$$\Omega_{CaCO_3} = \left[Ca^{2+}\right]\left[CO_3^{2-}\right]/K^*_{sp}$$

where $[Ca^{2+}]$ is the calcium ion concentration and K^*_{sp} is the stoichiometric solubility product, which increases with decreasing temperature and increasing pressure. Since the residence time of calcium is on the order of a million years, ocean Ω_{CaCO_3} will be decreased by ocean acidification over the coming centuries. Prior modeling studies have suggested that many areas in the water column, particularly the high-latitude oceans, will become undersaturated with respect to calcite and/or aragonite, two different polymorphs of $CaCO_3$ (Caldeira and Wickett, 2005; Orr et al., 2005; Andersson et al., 2006; Lenton and Britton, 2006; Cao et al., 2007; Cao and Caldeira, 2008).

Calcifying marine life, such as cocolithophores and foraminifera, may be vulnerable to those predicted changes in Ω_{CaCO_3} brought on by ocean acidification (Barker et al., 2003; Doney et al., 2009; Gehlen et al., 2007; Hofmann and Schellnhuber, 2009;

BGD
8, 11863–11897, 2011

SCBD, 2009; Turley et al., 2006; Tyrell, 2008; Zondervan et al., 2001). However, there is large variability in the calcifying response to acidification between species (Doney, 2009; Doney et al., 2009; Fabry et al., 2008; Guinotte and Fabry, 2008; Riebesell et al., 2000, 2007; Iglesias-Rodriguez et al., 2008). Decreased biogenic calcification ultimately leads to an increased ocean uptake of anthropogenic atmospheric CO_2 and a negative feedback on rising CO_2 levels offsetting the decreased ocean CO_2 uptake capacity resulting from acidification (Hofmann and Schellnhuber, 2009; Raven and Falkowski, 2000; Zondervan et al., 2001; Feely et al., 2004; Orr et al., 2005; Gehlen et al., 2008; Doney et al., 2009; Gangsto et al., 2011); however, the variability in species specific responses introduces a large uncertainty to predictions of how this feedback will operate in the future (Doney, 2009; Doney et al., 2009).

In addition to the uncertainty in species-specific responses to acidification, significant changes in ocean ecosystems are expected to arise from ocean warming (Doney, 2010; Schmittner et al., 2008). Among these, the temperature-dependence of plankton growth is expected to increase primary production in the ocean as the surface ocean warms (Schmittner et al., 2008). Because organic matter is recycled in the upper ocean much more efficiently than $CaCO_3$, this would be expected to result in an increase of the export of inorganic $CaCO_3$ particles relative to that of organic carbon. Moreover, the fact that organic export is more readily limited by nutrient supply could allow $CaCO_3$ export to significantly outstrip organic matter export in a warmer ocean, where recycled nutrients drive production. Thus, more rapid production of $CaCO_3$ due to higher temperatures (Schmittner et al., 2008) could potentially counteract the effect of acidification on calcification. The result has important implications for oceanic carbon storage.

The oceans have taken up approximately 30–40 % of anthropogenic CO_2 in the last 200 yr (Raven and Falkowski, 2000; Feely et al., 2004; Sabine et al., 2004; Zeebe et al., 2008). As $CaCO_3$ production uses up 2 moles of alkalinity per mole of DIC, a reduction in production would lead to a greater increase in surface water alkalinity than DIC; this, in turn, would result in a decrease in the Revelle factor of the surface ocean and a greater oceanic capacity to uptake atmospheric CO_2. The Revelle factor,

BGD
8, 11863–11897, 2011

or buffer factor, of the ocean describes how the pCO_2 of seawater changes for a given change in [DIC] as per

$$\text{Revelle Factor} = (\Delta[CO_2]/[CO_2])/(\Delta[DIC]/[DIC])$$

and its value is proportional to the ratio of sea surface DIC : alkalinity. As such, the ocean capacity to uptake atmospheric CO_2 is inversely proportional to the Revelle factor (Denman et al., 2007; Sabine et al., 2004). Neglecting mineral ballasting, a reduction in calcification may also reduce the rain ratio of particulate inorganic carbon to particulate organic carbon (PIC : POC) reaching the sediments. This would lead to greater metabolic dissolution of sedimentary $CaCO_3$, brought on by the increased organic matter decomposition acidifying sediment pore water, further altering of the vertical alkalinity and DIC gradients as well as the strength of the ocean as a carbon sink (Barker et al., 2003; Feely et al., 2004; Orr et al., 2005; Riebesell et al., 2007; Wolf-Gladrow et al., 1999; Zondervan et al., 2001). Changes in deep ocean saturation state brought on by the invasion of anthropogenic CO_2 in the deep ocean can also directly enhance the dissolution of $CaCO_3$ in sediments (Lenton and Britton, 2006). This increased dissolution of sedimentary $CaCO_3$ adds alkalinity to the ocean thereby reducing sea surface pCO_2 and further stimulating ocean carbon uptake on millennial timescales (Ridgwell and Hargreaves, 2007).

Several recent modeling studies have been conducted to examine changes in $CaCO_3$ production rates due to acidification and their effect on the fate of anthropogenic CO_2 (Heinze, 2004; Andersson et al., 2006; Gehlen et al., 2007; Gangsto et al., 2008). Despite significant research attention, however, estimates of the current rate of global $CaCO_3$ production vary widely: from 0.4 to 1.8 Pg C y^{-1} (Doney et al., 2009). Estimates of the calcification response to ocean acidification are even more uncertain. For example, Gangsto et al. (2008) simulated a 19 % calcification decrease by 2100 in an intermediate complexity climate model. In contrast, Andersson et al. (2006) simulated a 90 % decrease in calcification by 2300, using a box model driven by "business-as-usual" CO_2 emissions. Much of this variability is attributed to the calcifying species

BGD
8, 11863–11897, 2011

represented in the model, most often the coccolithophore *Emiliania huxleyi*. Consequently, other modeling studies have sought to address the inter-species/strain uncertainty in calcification response by comparing different calcification response scenarios. These studies have found that increased sensitivity of $CaCO_3$ production to changes in Ω_{CaCO_3} resulted in increased sea surface alkalinity (Ilynia et al., 2009), increased carbon sequestration, and decreased atmospheric pCO_2 (Ridgwell et al., 2006; Gangsto et al., 2011). Although studies agree that the acidification-calcification-CO_2 feedback is relatively small (Zondervan et al., 2001; Ridgwell et al., 2006; Gangsto et al., 2011), it still contributes uncertainty to climate model predictions. Consequently, it is critical that this feedback be properly represented in modeling studies, especially on centennial and longer timescales. It is also important to note that most modeling studies addressing the calcification-CO_2 feedback uncertainty are either conducted on centennial timescales or omit deep-sea carbonate sediment dynamics and so longer-term studies using models with deep-sea sediment components are required. Moreover, most studies of future $CaCO_3$ production projections focused only on ocean acidification effects and neglected the temperature effect, although both may be similarly important for long-term ocean carbon cycle changes.

The purpose of this study is to expand on the work of Ridgwell et al. (2006), Ilynia et al. (2009), and Gangsto et al. (2011) by: 1) incorporating a $CaCO_3$ production rate dependence on ocean calcite saturation state into an intermediate complexity climate model; 2) exploring a range of calcification responses, reflecting experimental uncertainty in the biogenic calcification response to increasing ocean carbon uptake; 3) comparing acidification and temperature effects on future $CaCO_3$ production; 4) evaluating different model solutions with modern observations; and 5) assessing the resulting impact on the magnitude and direction of future ocean carbon-climate feedbacks on millennial timescales. We conduct a series of model simulations, following two 21st century CO_2 emissions scenarios, and continue the simulations until the year 3500 following a cessation of anthropogenic CO_2 emissions in year 2100. These response scenarios are compared to the standard configuration of the model in order

BGD
8, 11863–11897, 2011

to determine the impact of changing marine calcification on ocean chemistry and the uptake of anthropogenic CO_2 on millennial timescales.

2 Materials and methods

2.1 Model description

The University of Victoria Earth System Climate Model (UVic ESCM) version 2.9 is an intermediate complexity global climate model with a spherical grid resolution of 1.8° latitude by 3.6° longitude. The climate component of the model consists of a simplified energy-moisture balance atmospheric model with dynamical feedbacks, coupled to a primitive equation three-dimensional ocean general circulation model (Modular Ocean Model 2 or MOM2), and a thermodynamic/dynamic sea ice model (Weaver et al., 2001). The carbon cycle component of the model is represented by a dynamic vegetation model (Top-down Representation of Interactive Foliage and Flora Including Dynamics or TRIFFID) (Cox, 2001; Meissner et al., 2003), a land surface model (a simplified version of the Met Office Surface Exchange Scheme or MOSES) (Meissner et al., 2003), an ocean ecosystem/biogeochemical model and an inorganic ocean carbon model (Schmittner et al., 2008), and an oxic-only model of ocean sediment respiration (Archer, 1996; Eby et al., 2009).

The MOM2 ocean component includes numerous physical parameterizations such as diffusive mixing along and between layers of different water density, eddy induced tracer transport based on Gent and McWilliams (1990), and the computation of tidally induced diapycnal mixing over rough seafloor topography (Simmons et al., 2004). Radiocarbon ^{14}C and chlorofluorocarbons (CFCs) are used to track the ocean's ventilation to the atmosphere on decadal to millennial scales (Schmittner et al., 2008). The inorganic carbon cycle model is an Ocean Carbon-Cycle Intercomparison type (OCMIP-2) model while the ocean ecosystem/biogeochemical model is a nutrient-phytoplankton-zooplankton-detritus (NPZD) model based on Schmittner et al. (2005) with a fast microbial-induced nutrient recycling parameterization based on Schartau and Oschlies (2003). The NPZD model further includes two kinds of phytoplankton (nitrogen fixers

BGD
8, 11863–11897, 2011

and other phytoplankton (P_o)), nutrients such as phosphate (PO_4) and nitrate (NO_3), and tracers such as DIC, alkalinity, and oxygen (O_2).

The production of $CaCO_3$ in the model is calculated as

$$Pr(CaCO_3) = ((1-\beta)G(P_o)Z + \mu_{P2}P_o^2 + \mu_z Z^2)(PIC^* : POC^*)R_{C:P}$$

where $(1-\beta)G(P_o)Z$ represents the zooplankton grazing of the P_o phytoplankton type, $\mu_{P2}P_o^2$ represents the mortality of P_o phytoplankton, $\mu_z Z^2$ represents zooplankton mortality, ($PIC^* : POC^*$) is the production ratio of $CaCO_3$ to particulate organic carbon, and $R_{C:P}$ is the molar elemental ratio of carbon to phosphorus. As the vertically integrated $CaCO_3$ (PIC) production in the model is parameterized as a fixed ratio of the production of nondiazotrophic detritus (POC), the strength of the $CaCO_3$-pump is strongly influenced by the $PIC^* : POC^*$ parameter. The dissolution of $CaCO_3$ in the water column assumes an instantaneous sinking of the vertically integrated production (Schmittner et al., 2008) with an e-folding depth of 6500 m.

Phytoplankton growth rates and microbial remineralization rates in the biological carbon cycle component are assumed to increase with increasing temperature (Eppley, 1972; Schmittner et al., 2008). Consequently, detrital production rates increase with increasing temperature as well due to enhanced biological carbon fixation. As $CaCO_3$ production in the model is parameterized as a fixed ratio of nondiazotrophic detrital production (the $PIC^* : POC^*$ parameter), $CaCO_3$ production rates tend to increase along with detrital production rates in response to increasing sea surface temperatures resulting in a stronger vertical ocean alkalinity gradient (Schmittner et al., 2008).

The marine sediment component consists of 13 layers ranging from a few millimeters near the sediment surface to a few centimeters at the bottom of the domain at a depth of 10 cm. The penetration depth of POC into the surface sediment mixed layer in contact with overlying bottom waters, or "pore layer", is determined by the balance between the respiration rate constant and the sediment-mixing rate. Sediment $CaCO_3$ dissolution is regulated by the kinetics of diffusion of the dissolved reaction products from the sediments to the overlying water while the concentration and burial rates of

BGD
8, 11863–11897, 2011

sedimentary $CaCO_3$ are predicted using the PIC : POC rain ratio, dilutant burial rates (primarily clay and opal), and the reaction rate laws for both organic carbon and $CaCO_3$ (Archer, 1996). Only oxic metabolic dissolution of sedimentary $CaCO_3$ is simulated by the sediment component and the effects of suboxic and anoxic metabolism are not accounted for (Eby et al., 2009).

It should be noted that the UVic ESCM does not differentiate between the different polymorphs of $CaCO_3$ such as aragonite and calcite. Since the model does not properly resolve coastal processes where aragonite is produced we focus on the dependence of calcification on calcite saturation state only (Ω_{CaCO_3}), which is a reasonable approximation given that approximately 90 % of pelagic calcification is in the form of calcite (Fabry, 1990). Furthermore, mineral ballasting, which increases the efficiency of POC export to the deep sea, is not represented in the UVic ESCM therefore the model assumes an independence of organic and inorganic material fluxes to the deep ocean. Finally, for the purposes of this study, we have focused on the production dependence on Ω_{CaCO_3}, and have not also introduced a dependence of dissolution on Ω_{CaCO_3}.

2.2 Model experimental methodology

We present a series of transient model simulations from the year 1800 to 3500, so as to reasonably cover one full cycle of the oceanic meridional overturning circulation. In order to achieve a stable preindustrial climate, all model configurations were individually integrated for 10 000 model years using fixed preindustrial boundary conditions. Transient runs are categorized in two suites of six simulations each. The first suite (suite S) was forced by the Intergovernmental Panel on Climate Change's "business-as-usual" SRES A2 CO_2 emissions scenario, reaching cumulative CO_2 emissions of 2166 Pg C by the year 2100. After 2100, emissions were set to zero for the duration of the simulations. The second suite (suite M) was forced by a "mitigation" emissions scenario, in which emissions peaked in the year 2020 and decreased to zero in year 2100, such that cumulative CO_2 emissions were 1000 Pg C.

BGD
8, 11863–11897, 2011

Within each suite (S and M), we carried out six simulations, each with an increasing sensitivity of $CaCO_3$ production to changes in Ω_{CaCO_3} (Fig. 1). In the standard model configuration, $CaCO_3$ production is independent of saturation state and the PIC : POC production ratio used in the calculation of $CaCO_3$ production is fixed at a value of 0.018. This configuration was used for the "control" simulations S0 and M0 (see Table 1) and represents only the temperature effect on $CaCO_3$ production (Schmittner et al., 2008). In the simulations with $CaCO_3$ production-saturation state dependence (S1 to S5 and M1 to M5 in Table 1), we introduced a Michaelis-Menten function to calculate the $CaCO_3$: nondiazotrophic detritus production ratio (PIC : POC) as a function of saturation state (Ω):

$$\left(\frac{\mathrm{PIC}}{\mathrm{POC}}\right) = \left(\frac{\mathrm{PIC}}{\mathrm{POC}}\right)_{\max} \times \left(\frac{(\Omega - 1)}{K_{\max} + (\Omega - 1)}\right)$$

In this relationship, $(\mathrm{PIC/POC})_{\max}$ is a specified maximum production ratio, and $K_{\max}$ is a half-saturation constant defining the value of $(\Omega - 1)$ for which PIC/POC equals one half of $(\mathrm{PIC/POC})_{\max}$ (Gehlen et al., 2007).

Table 1 summarizes the values of $(\mathrm{PIC : POC})_{\max}$ and $K_{\max}$ used for each model version. We selected values of $K_{\max}$ ranging from 0.07 to 20 for each scenario in order to vary the shape of the PIC : POC vs. Ω_{CaCO_3} function between no PIC : POC – Ω_{CaCO_3} response (scenario 0) to a near linear response (scenario 5), as illustrated in Fig. 1. In order to keep the global preindustrial PIC : POC production ration the same in all models, we back-calculated the value for $(\mathrm{PIC : POC})_{\max}$ in each scenario using the global mean preindustrial sea-surface calcite saturation state value of 4.78 from the standard model. In the subsequent transient simulations, changes to the PIC : POC production ratio over time brought about by ocean acidification varied according to the imposed calcification sensitivities.

Alkalinity is removed from the ocean by permanent burial in sediments, and added to the ocean by dissolution of the active calcite sediment layer and by a weathering flux from land. In all simulations the weathering flux was held constant.

BGD
8, 11863–11897, 2011

3 Results

The modern $CaCO_3$ production rate of 0.6 Pg C y^{-1} predicted in the standard version of the model falls within the estimates of 0.6–1.6 Pg C y^{-1} based on satellite and sediment trap data and of 0.4–1.8 Pg C y^{-1} based on model predictions (Doney et al., 2009). The rain ratio of $CaCO_3$: POC across 130-m depth for all six model configurations is shown in Fig. 2. The global mean rain ratio for all six model configurations is 0.06 which is consistent with observational estimates of 0.06 ± 0.03 (Sarmiento et al., 2002) and is comparable to the range of 0.07–0.11 established in other studies (Lee, 2001; Jin et al., 2006). The mean rain ratio across the Atlantic, Pacific, and Indian Oceans is also consistent with observational estimates (Sarmiento et al., 2002; Jin et al., 2006). Overall, the rain ratio exhibits a strong latitudinal dependence with lower global mean ratios at high latitudes. This latitudinal dependence is dominated by the temperature-effect on recycling, as indicated by the relatively small differences between the six saturation-state dependent scenarios. Nonetheless, increasing sensitivity of $CaCO_3$ production to Ω_{CaCO_3} increases the latitudinal dependence of the rain ratio. The errors and differences between the observational estimates are typically larger than the differences between the different model versions, which render the observations of little use in constraining the models.

Higher rain ratios at low latitudes lead to more efficient removal of alkalinity from the tropical surface ocean (Fig. 3). The control model (S0) captures the spatial patterns of high surface potential alkalinity at high latitudes and along the eastern boundary of the Pacific and low values elsewhere, although the observed gradients are slightly overestimated. Models with high sensitivity of $CaCO_3$ production to Ω_{CaCO_3} increase the gradients even more making the agreement with the observations worse.

A comparison of modeled ocean alkalinity and DIC in the year 1995 with gridded data sets based on field measurements in the 1990's (Key et al., 2004) is shown in Fig. 4. The UVic model version 2.9 contains an average of 59 mmol m^{-3} more alkalinity than the observations, due to errors in the burial flux of $CaCO_3$. In addition, the

BGD
8, 11863–11897, 2011

model simulates a somewhat stronger alkalinity pump than observed, evidenced by high simulated alkalinity in the deep North Pacific. There is little difference between the standard configuration of the model (run S0) and the extreme calcification-sensitivity configuration (run S5) relative to both each other and GLODAP observations. Run S5 has higher alkalinity values in the deep ocean, particularly in the northern hemisphere, increasing the difference with the observations compared to run S0. In Southern Ocean bottom waters, on the other hand, values are lower and in better agreement with the observations compared to S0. Zonally averaged DIC concentrations are almost indistinguishable in the different models.

In the standard "business as usual" simulation (run S0), total ocean carbon increased by 517 Pg C by 2100, resulting in maximum decreases of globally averaged surface pH and surface Ω_{CaCO_3} of 0.397 and 2.34 respectively near year 2100 (Fig. 5). In the standard "mitigation" run M0, the reductions of sea surface pH and Ω_{CaCO_3} were much less, reaching maximal decreases of 0.175 and 1.19 respectively relative near 2100 (Fig. 5). In both cases, after CO_2 emissions ceased in the year 2100, ocean surface pH and saturation state rapidly stabilized and began slow recoveries. For the remainder of the discussion, we focus only on the business-as-usual simulations, given that the mitigation runs generally show the same patterns of variability but with smaller magnitudes, though information for both types of simulations are shown in the tables.

Varying the sensitivity of $CaCO_3$ production to decreasing Ω_{CaCO_3} had a dramatic effect on the response of $CaCO_3$ production rates to increased ocean carbon uptake. In the run with no dependence on saturation state (S0) the $CaCO_3$ production rate increased by as much as $\sim 0.18\,Pg\,C\,y^{-1}$, an increase of $\sim 20\,\%$ relative to the preindustrial state (Fig. 6). In contrast, the strongest response to acidification (S5) caused an opposite response, with $CaCO_3$ production decreasing by almost $0.3\,Pg\,C\,y^{-1}$, a decrease of more than 30 %. Simulation S3, with an intermediate dependence on saturation state, produced a cancellation between the temperature and acidification responses leading to a near-constant production rate of $CaCO_3$.

BGD
8, 11863–11897, 2011

In simulations that included an acidification sensitivity (S1–S5), decreased $CaCO_3$ production led to weaker vertical gradients of alkalinity and DIC with increased concentrations at the surface and decreased concentrations at depth relative to control (Fig. 7). The greatest increases in alkalinity and DIC occurred in the thermocline and throughout the water column in the Arctic Ocean. Throughout most of the ocean, DIC and alkalinity decreased at depth as a result of decreased export of particulate inorganic carbon to the deep ocean, with the largest decreases evident at around 60° S and 45° N.

As shown in Fig. 8, the simulations show a large volume of the ocean falling below calcite saturation ($\Omega < 1$), extending to about 500 m depth in the equatorial region and in the high latitude Southern Oceans in the zonal average. Compared to the control simulation (S0), runs with acidification-sensitive calcification showed more severe undersaturation developing in the deep sea, and reduced acidification throughout the thermocline, due to weakening of the alkalinity pump.

The sedimentary $CaCO_3$ pool also responded to the calcifer sensitivity to acidification, affecting the global alkalinity inventory. In the control run, the PIC : POC rain ratio at the ocean sediments rose over time as a result of temperature effect on $CaCO_3$ production rates (Fig. 9). This rise was dampened by increasing sensitivity of calcification to acidification, with the most sensitive runs (S4 and S5) showing temporary decreases in the rain ratio below the initial rain ratio. But despite any increases in the rain ratio, the global mass of $CaCO_3$ sediment in the active layer decreased in all cases, due to dissolution by acidic bottom waters. The burial rate of $CaCO_3$ sediments decreased with increasing sensitivity of calcifiers to acidification, because of the relatively smaller flux of $CaCO_3$ to the sediments (Fig. 9, Table 5).

4 Discussion

In the absence of the Ω_{CaCO_3}-effect (runs S0 and M0), $CaCO_3$ production increased proportionally with the temperature-dependent primary production rate, as shown by

BGD
8, 11863–11897, 2011

Schmittner et al. (2008). This occurs despite a small decrease in the globally-averaged surface PO_4 concentration (not shown) due to greater recycling of nutrients and higher intrinsic growth rates (Eppley, 1971). In configurations 1 and 2, the sensitivity of $CaCO_3$ production rates to changes in Ω_{CaCO_3} was not high enough to completely counteract this temperature effect. Thus, although reduced relative to control, $CaCO_3$ production rates in these configurations increased between years 1800 and 2100 despite increasing ocean acidification. In configurations 3–5, however, the sensitivity of $CaCO_3$ production rates to changes in Ω_{CaCO_3} was high enough to counteract this temperature effect resulting in decreases in $CaCO_3$ production rates between years 1800 and 2100. In the most extreme case, the globally integrated $CaCO_3$ production of configuration S0 was 30 % higher than that of S5 in the year 2100.

The $CaCO_3$ pump representation in the UVic ESCM is fairly simple (e.g. there is no distinction between the different polymorphs of $CaCO_3$). Nonetheless, the results generally agree with other similar studies in that increasing acidification lead to a reduction in $CaCO_3$ production rates, to a degree dependent on the sensitivity of calcifiers to saturation state (Andrersson et al., 2006; Gangsto et al., 2008, 2011; Gehlen et al., 2007; Heinze, 2004; Ridgwell et al., 2006; SCBD, 2009). The important dynamic highlighted here – the opposing effects of increasing growth rates vs. decreasing calcification – depends equally on the complex response of ocean ecosystems to recycling of nutrients in the surface layer, and the myriad controls on export. It is difficult to evaluate to what degree the model represents these processes properly, given the current state of understanding, but it is also certain to vary between models. Tentative comparison to surface potential alkalinity observations (Fig. 3) indicates that these observations could be used in the future to better constrain the relative importance of the temperature versus the acidification effect. Our results emphasize that temperature-driven changes may be of equal or greater importance to acidification in determining future pelagic $CaCO_3$ production.

In our simulations, carbon is redistributed differently amongst the atmospheric, ocean, and sediment reservoirs dependent on the varying $CaCO_3$ production rates.

BGD
8, 11863–11897, 2011

In all simulations, decreasing $CaCO_3$ production rates resulted in greater carbon uptake by the ocean and a reduced airborne fraction of carbon. Between years 1800 and 3500, atmospheric pCO_2 decreased by 2.81–52.2 ppmv in runs S1–S5 (and by 0.377–11.2 ppmv in runs M1–M5) relative to control, a similar magnitude to that estimated by Barker et al. (2003), Heinze et al. (2004), Gehlen et al. (2007). It is interesting to note that the net increase of the ocean carbon reservoir exceeds the decrease of the atmospheric carbon reservoir (Tables 2 and 3). The carbon that makes up the difference originates from the terrestrial and marine sediment carbon reservoirs. The sediment reservoir, in particular, adds carbon to the ocean due to $CaCO_3$-sediment dissolution. This highlights the importance of including inter-active terrestrial carbon and sediment carbon components when assessing the CO_2-$CaCO_3$ climate feedback.

The downward flux of $CaCO_3$ from the sediment pore layer followed the same pattern as $CaCO_3$ production rates seen in the S simulations and decreased relative to simulation S0 with greater sensitivity of $CaCO_3$ production to Ω_{CaCO_3}. Consequently, the decrease in rain ratio contributed to both a reduction of $CaCO_3$ in the pore-layer and decreased accumulation of $CaCO_3$ in deeper sediments (Table 4). We note that inclusion of the ballast-effect of $CaCO_3$ on settling organic matter fluxes (Armstrong, 2002) would likely decrease the sensitivity of $CaCO_3$ burial to the $CaCO_3$ export flux, by reducing the variability in sediment rain ratios.

5 Conclusions

Ocean acidification is a growing concern in the scientific community. Its impact on calcifying marine life shows high inter-species variability, and the subsequent changes to marine carbon cycling contribute uncertainty to climate model predictions of future climate change and the fate of anthropogenic CO_2.

A number of modeling studies have attempted to address this uncertainty by assessing a range of biogenic calcification responses to changes in $CaCO_3$ saturation state rather than relying on the single-calcifier species representation commonly found

BGD
8, 11863–11897, 2011

in many ocean ecosystem/biogeochemical models (Ridgwell et al., 2006; Ilynia et al., 2009; Gangsto et al., 2011). Our research has applied a broadly similar approach by implementing a new dependence of $CaCO_3$ production rates on calcite saturation state to a coupled carbon-climate model. We used six model configurations: one control configuration where $CaCO_3$ production rates remained independent of saturation state and five calcification response configurations with increasing sensitivity of production rates to saturation state changes. These configurations were forced by two different CO_2 emissions scenarios allowing us to assess the differences in carbon partitioning between the various reservoirs, alkalinity and dissolved inorganic carbon distribution, and the strength of the ocean carbon sink.

Our simulations show that the response of the UVic ESCM's marine $CaCO_3$ cycle to anthropogenic CO_2 hinges on the degree to which increased temperatures accelerate plankton growth, vs. the degree to which acidification hinders calcification. Greater sensitivity to acidification shifts carbon partitioning between atmosphere, ocean, and marine sediments by weakening the vertical ocean alkalinity and DIC gradients and decreasing sediment burial of $CaCO_3$. Both of these effects increase surface ocean alkalinity. As a result, ocean carbon uptake is enhanced, acting as a negative feedback on rising atmospheric CO_2 of approximately 13 %, producing an equivalent decrease in warming by year 3500 of 13 % (0.4 °C). In the absence of a strong sensitivity of calcifiers to acidification, the climate feedback on the carbon cycle is positive, increasing the airborne fraction of carbon as the ocean warms (Schmittner et al., 2008). It appears that the effect of the $CaCO_3$ production-Ω_{CaCO_3} relationship on the marine carbon cycle is significant for future climate projections, on the millennial timescale. This effect is in addition to the serious effects that acidification is expected to have on pelagic and coastal biota. Improving the representation of long-term carbon-cycle processes in models will help us to quantify and evaluate the millennial-scale climate legacy that we may bequeath to future generations.

BGD
8, 11863–11897, 2011

Acknowledgements. This study was funded by HDM's *Nouveaux Chercheurs* grant from the Fonds Québécois de la Recherche sur la Nature et la Technologie, the National Science and Engineering Research Council of Canada, the Canadian Foundation for Climate and Atmospheric Sciences, the Global Environmental and Climate Change Center, and Concordia University.

References

Archer, D.: A data-driven model of the global calcite lysocline, Global Biogeochem. Cy., 10(3), 511–526, 1996.

Andersson, A. J., Mackenzie F. T., and Lerman, A.: Coastal ocean CO_2-carbonic acid-carbonate sediment system of the Anthropocene, Global Biogeochem. Cy., 20(1), GB1S92, doi:10.1029/2005GB002506, 2006.

Barker, S., Higgins, J. A., and Elderfield, H.: The future of the carbon cycle: review, calcification response, ballast and feedback on atmospheric CO_2, Philos. T. R. Soc. A, 361(1810), 1977–1998, 2003.

Cao, L. and Caldeira, K.: Atmospheric CO_2 stabilization and ocean acidification, Geophys. Res. Lett., 35(19), L19609, doi:10.1029/2008GL035072, 2008.

Cao, L., Caldeira, K., and Jain, A. K.: Effects of carbon dioxide and climate change on ocean acidification and carbonate mineral saturation, Geophys. Res. Lett., 34(5), L05607, doi:2006GL028605, 2007.

Caldeira, K. and Wickett, M. E.: Ocean model predictions of chemistry changes from carbon dioxide emissions to the atmosphere and ocean, J. Geophys. Res.-Oceans, 110, C09S04, doi:10.1029/2004JC002671, 2005.

Cox, P. M.: Description of the "TRIFFID" dynamic global vegetation model, Hadley Center Technical Note 24, Met Office, Exeter, UK, 2001.

Denman, K. L., Brasseur, G., Chidthaisong, A., Ciais, P., Cox, P. M., Dickinson, R. E., Hauglustaine, D., Heinze, C., Holland, E., Jacob, D., Lohmann, U., Ramachandran, S., Da Silva Dias, P. L., Wofsy, S. C., and Zhang, X.: Couplings between changes in the climate system and biogeochemistry, in: Climate Change 2007: The Physical Science Basis. Contribution of Working Group I to the Fourth Assessment Report of the Intergovernmental Panel on Climate Change, edited by: Solomon, S., Qin, D., Manning, M., Chen, Z., Marquis, M., Averyt, K. B.,

BGD

8, 11863–11897, 2011

Tignor, M., and Miller, H. L., Cambridge University Press, Cambridge, UK and New York, NY, USA, 2007.
Doney, S. C.: The consequences of human-driven ocean acidification for marine life, Biology Reports Ltd., 1(36), doi:10.3410/B1-36, 2009.
Doney, S. C.: The growing human footprint on coastal and open-ocean biogeochemistry, Science, 328(5985), 1512–1516: doi:10.1126/science.1185198, 2010.
Doney, S. C., Fabry, V. J., Feely, R. A., and Kleypas, J. A.: Ocean acidification: the other CO_2 problem, Annu. Rev. Marine Sci., 1, 169–192, 2009.
Eby, M., Zickfeld, K., Montenegro, A., Archer, D., Meissner, K. J., and Weaver, A. J.: Lifetime of Anthropogenic climate change: millennial time scales of potential CO_2 and surface temperature perturbations, J. Climate, 22(10), 2501–2511, 2009.
Eppley, R. W.: Temperature and phytoplankton growth in the sea, Fish. B.-NOAA, 70, 1063–1085, 1972.
Fabry, V. J.: Shell growth rates of pteropod and heteropod mollusks and aragonite production in the open ocean: Implications for the marine carbonate system, J. Mar. Res., 48, 209–222, 1990.
Fabry, V. J., Seibel, B. A., Feely, R. A., and Orr, J. C.: Impacts of ocean acidification on marine fauna and ecosystem processes, ICES J. Mar. Sci., 65, 414–432, 2008.
Falkowski, P., Scholes, R. J., Boyle, E., Canadell, J., Canfield, D., Elser, J., Gruber, N., Hibbard, K., Högberg, P., Linder, S., Mackenzie, F. T., Moore III, B., Pendersen, T., Rosenthal, Y., Seitzinger, S., Smetacek, V., and Steffen, W.: The global carbon cycle: a test of our knowledge of earth as a system, Science, 290(5490), 291–296, 2000.
Feely, R. A., Sabine, C. L., Lee, K., Berelson, W., Kleypas, J., Fabry, V. J., Millero, F. J.: Impact of anthropogenic CO_2 on the $CaCO_3$ system in the oceans, Science, 305(5682), 362–366, 2004.
Feely, R. A., Sabine, C. L., Hernandez-Ayon, J. M., Lanson, D., and Hales, B.: Evidence for upwelling of corrosive "acidified" water into the continental shelf, Science, 320(5882), 1490–1492, 2008.
Gangstø, R., Gehlen, M., Schneider, B., Bopp, L., Aumont, O., and Joos, F.: Modeling the marine aragonite cycle: changes under rising carbon dioxide and its role in shallow water $CaCO_3$ dissolution, Biogeosciences, 5, 1057–1072, doi:10.5194/bg-5-1057-2008, 2008.
Gangstø, R., Joos, F., and Gehlen, M.: Sensitivity of pelagic calcification to ocean acidification, Biogeosciences, 8, 433–458, doi:10.5194/bg-8-433-2011, 2011.

BGD
8, 11863–11897, 2011

Gehlen, M., Gangstø, R., Schneider, B., Bopp, L., Aumont, O., and Ethe, C.: The fate of pelagic $CaCO_3$ production in a high CO_2 ocean: a model study, Biogeosciences, 4, 505–519, doi:10.5194/bg-4-505-2007, 2007.

Gehlen, M., Bopp, L., and Aumont, O.: Short-term dissolution response of pelagic carbonate sediments to the invasion of anthropogenic CO_2: A model study, Geochem. Geophy. Geosy., 9, Q02012, doi:10.1029/2007GC001756, 2008.

Gent, P. R. and McWilliams, J. C.: Isopycnal mixing in ocean circulation models, J. Phys. Oceanogr., 20(1), 150–155, 1990.

Heinze, C.: Simulating oceanic $CaCO_3$ export production in the greenhouse, Geophys. Res. Lett., 31(16), L16308, doi:10.1029/2004GL020613, 2004.

Hofmann, M. and Schellnhuber, H.: Oceanic acidification affects marine carbon pump and triggers extended marine oxygen holes, P. Natl. Acad. Sci. USA, 106(9), 3017–3022, 2009.

Iglesias-Rodriguez, M. D., Halloran, P. R., Rickaby, R. E. M., Hall, I. R., Colmenero-Hidalgo, E., Gittins, J. R., Green, D. R. H., Tyrrell, T., Gibbs, S. J., Von Dassow, P., Rehm, E., Armbrust, E. V., and Boessenkool, K. P.: Phytoplankton calcification in a high-CO_2 world, Science, 320(5874), 336–340, 2008.

Ilynia, T., Zeebe, R. E., Maier-Reimer, E., and Heinze, C.: Early detection of ocean acidification effects on marine calcification, Global Biogeochem. Cy., 23, GB1008, doi:10.1029/2008GB003278, 2009.

Jin, X., Gruber, N., Dunne, J. P., Sarmiento, J. L., and Armstrong, R. A.: Diagnosing the contribution of phytoplankton functional groups to the production and export of particulate organic carbon, $CaCO_3$, and opal from global nutrient and alkalinity distributions, Global Biogeochem. Cy., 20, GB2015, doi:10.1029/2005GB002532, 2006.

Key, R. M., Kozyr, A., Sabine, C. L., Lee, K., Wanninkhof, R., Bullister, J. L., Feely, R. A., Millero, F. J., Mordy, C., and Peng, T.-H.: A global ocean carbon climatology: Results from the global data analysis project (GLODAP), Global Biogeochem. Cy., 18, GB4031, doi:10.1029/2004GB002247, 2004.

Lee, K.: Global net community production estimated from the annual cycle of surface water total dissolved inorganic carbon, Limnol. Oceanogr., 46(6), 1287–1297, 2001.

Lenton, T. M. and Britton, C.: Enhanced carbonate and silicate weathering accelerates recovery from fossil fuel CO_2 perturbations, Global Biogeochem. Cy., 20(3), GB3009, doi:10.1029/2005GB002678, 2006.

Meissner, K. J., Weaver, A. J., Matthews, H. D., and Cox, P. M.: The role of land-surface

BGD
8, 11863–11897, 2011

dynamics in glacial inception: a study with the UVic Earth System Climate Model, Clim. Dynam., 21, 515–537, 2003.
Orr, J. C., Fabry, V. J., Aumont, O., Bopp, L., Doney, S. C., Feely, R. A., Gnanadesikan, A., Gruber, N., Ishida, A., Joos, F., Key, R. M., Lindsay, K., Maier-Reimer, E., Matear, R., Monfray, P., Mouchet, A., Najjar, R. G., Plattner, G., Rodgers, K. B., Sabine, C. L., Sarmiento, J. L., Schlitzer, R., Slater, R. D., Totterdell, I. J., Weirig, M., Yamanaka, Y., and Yool, Y.: Anthropogenic ocean acidification over the twenty-first century and its impact on calcifying organisms, Nature, 437(7059), 681–686, 2005.
Raven, J. A. and Falkowski, P. G.: Oceanic sinks for atmospheric CO_2, Plant Cell Environ., 22(6), 741–755, 1999.
Ridgwell, A. and Hargreaves, J. C.: Regulation of atmospheric CO_2 by deep-sea sediments in an Earth system model, Global Biogeochem. Cy., 21(2), GB2008, doi:10.1029/2006GB002764, 2007.
Ridgwell, A., Zondervan, I., Hargreaves, J. C., Bijma, J., and Lenton, T. M.: Assessing the potential long-term increase of oceanic fossil fuel CO_2 uptake due to CO_2-calcification feedback, Biogeosciences, 4, 481–492, doi:10.5194/bg-4-481-2007, 2007.
Riebesell, U., Zondervan, I., Rost, B., Tortell, P. D., Zeebe, R. E., and Morel, F. M. M.: Reduced calcification of marine plankton in response to increased atmospheric CO_2, Nature, 407(6802), 364–367, 2000.
Riebesell, U., Schulz, K. G., Bellerby, R. G. J., Botros, M., Fritsche, P., Meyerhofer, M., Neill, C., Nondal, G., Oschlies, A., Wohlers, J., and Zöllner, E.: Enhanced biological carbon consumption in a high CO_2 ocean, Nature, 450(7169), 545–548, 2007.
Sabine, C. L., Feely, R. A., Gruber, N., Key, R. M., Lee, K., Bullister, J. L., Wanninkhof, R., Wong, C. S., Wallace, D. W. R., Tilbrook, B., Millero, F. J., Peng, T., Kozyr, A., Ono, T., and Rios, A.: The oceanic sink for anthropogenic CO_2, Science, 350(5682), 367–371, 2004.
Sarmiento, J. L., Dunne, J., Gnanadesikan, A., Key, R. R., Matsumoto, K., and Slater, R.: A new estimate of the $CaCO_3$ to organic carbon export ratio, Global Biogeochem. Cy., 16(4), 1107, doi:10.1029/2002GB001919, 2002.
Secretariat of the convention on biological diversity: Scientific Synthesis of the Impacts of Ocean Acidification on Marine Biodiversity, Technical Series No. 46, Montreal, 61 pp., 2009.
Schartau, M. and Oschlies, A.: Simultaneous data-based optimization of a 1D-ecosystem model at three locations in the North Atlantic, Part 1: Method and parameter estimates, J. Mar. Res., 61, 765–793, 2003.

BGD
8, 11863–11897, 2011

Schmittner, A., Oschlies, A., Giraud, X., Eby, M., and Simmons, H. L.: A global model of the marine ecosystem for long term simulations: sensitivity to ocean mixing, buoyancy forcing, particle sinking and dissolved organic matter cycling, Global Biogeochem. Cy., 19, GB3004, doi:10.1029/2004GB002283, 2005.

Schmittner, A., Oschlies, A., Matthews, H. D., and Galbraith, E. D.: Future changes in climate, ocean circulation, ecosystems, and biogeochemical cycling simulated for a business-as-usual CO_2 emission scenario until year 4000 AD, Global Biogeochem. Cy., 22(1), GB1013, doi:10.1029/2007GB002953, 2008.

Simmons, H. L., Jayne, S. R., St.Laurent, L. C., and Weaver, A. J.: Tidally driven mixing in a numerical model of the ocean general circulation, Ocean Model., 6(3–4), 245–263, 2004.

Turley, C., Blackford, J. C., Widdicombe, S., Lowe, D., Nightingale, P. D., and Rees, A. P.: Reviewing the impact of increased atmospheric CO_2 on oceanic pH and the marine ecosystem, in: Avoiding Dangerous Climate Change, edited by: Schellnhuber, H. J., Cramer, W., Nakicenovic, N., Wigley, T., and Yohe, G., 8. Cambridge University Press, Cambridge, 65–70, 2006.

Tyrrell, T.: Calcium carbonate cycling in future oceans and its influence on future climates, J. Plankton Res., 30(2), 141–156, 2008.

Weaver, A. J., Eby, M., Wiebe, E. C., Bitz, C. M., Duffy, P. B., Ewen, T. L., Fanning, A. F., Holland, M. M., Macfadyen, A., Matthews, H. D., Meissner, K. J., Saenko, O., Schmittner, A., Wang, H., and Yoshimori, M.: The UVic Earth System Climate Model: model description, climatology and applications to past, present and future climates, Atmos. Ocean., 39, 361–428, 2001.

Wolf-Gladrow, D. A., Riebesell, U., Burkhardt, S., and Bijma, J.: Direct effects of CO_2 concentration on growth and isotopic composition of marine plankton, Tellus B, 51(2), 461–476, 1999.

Zeebe, R. E., Zachos, J. C., Caldeira, K., and Tyrrell, T.: Oceans – carbon emissions and acidification, Science, 321(5885), 51–52, 2008.

Zondervan, I., Zeebe, R. E., Rost, B., and Riebesell, U.: Decreasing marine biogenic calcification: a negative feedback on rising atmospheric pCO_2, Global Biogeochem. Cy., 15(2), 507–516, 2001.

BGD
8, 11863–11897, 2011

Table 1. Summary of Model Run Calibrations.

Scenarios	Cumulative CO_2 Emissions by 2100 (Pg C)	K_{max}	$(PIC:POC)_{max}$	PIC : POC at Preindustrial Surface $\Omega_{calcite}$	Preindustrial Surface $\Omega_{calcite}$
S0		–	–		
S1		0.07	0.0183		
S2		0.5	0.0204		
S3	2166 Pg C (all S)	1.5	0.0251		
S4		3	0.0322		
S5		20	0.113		
M0		–	–	0.0180 (all)	4.78 (all)
M1		0.07	0.0183		
M2		0.5	0.0204		
M3	1000 Pg C (all M)	1.5	0.0251		
M4		3	0.0322		
M5		20	0.113		

BGD
8, 11863–11897, 2011

Table 2. Summary of the change in atmospheric and ocean output for years 1800–3500 for Suite S simulations. Values in column $S0_{1800}$ represent absolute output in the base model in year 1800. Subsequent columns show differences from 1800 to 3500 for each calcification sensitivity (S0 to S5).

	$S0_{1800}$	$S0_{3500-1800}$	$S1_{3500-1800}$	$S2_{3500-1800}$	$S3_{3500-1800}$	$S4_{3500-1800}$	$S5_{3500-1800}$
$CaCO_3$ Production Rate (Pg C y^{-1})	0.572	0.143	0.132	0.0776	0.0235	−0.0150	−0.0926
Sea Surface Alkalinity (Pg C)	175	−5.23	−4.98	−3.94	−2.71	−1.76	0.340
Sea Surface DIC (Pg C)	152	4.44	4.61	5.30	6.13	6.76	8.16
Sea Surface pCO_2 (ppmv)	293	316	313	302	290	281	263
Total Ocean Alkalinity (Pg C)	39 495	39.1	48.6	97.2	157	203	319
Total Ocean Carbon (Pg C)	37 321	1138	1150	1200	1260	1305	1410
Total Atmospheric Carbon (Pg C)	602	667	661	637	612	594	556
Sea Surface Calcite Saturation State	4.81	−1.81	−1.79	−1.73	−1.65	−1.59	−1.45
Sea Surface pH	8.16	−0.288	−0.286	−0.277	−0.267	−0.259	−0.242

BGD
8, 11863–11897, 2011

Table 3. Summary of the change in atmospheric and ocean output for years 1800–3500 for Suite M simulations. Values in column $M0_{1800}$ represent absolute output in the base model in year 1800. Subsequent columns show differences from 1800 to 3500 for each calcification sensitivity (M1 to M5).

	$M0_{1800}$	$M0_{3500-1800}$	$M1_{3500-1800}$	$M2_{3500-1800}$	$M3_{3500-1800}$	$M4_{3500-1800}$	$M5_{3500-1800}$
$CaCO_3$ Production Rate (Pg C y^{-1})	0.572	0.0615	0.0585	0.0436	0.0237	0.00752	−0.0286
Sea Surface Alkalinity (Pg C)	175	−2.31	−2.24	−1.95	−1.53	−1.17	−0.228
Sea Surface DIC (Pg C)	152	1.97	2.02	2.21	2.48	2.70	3.31
Sea Surface pCO_2 (ppmv)	293	104	103	102	99.4	97.4	92.4
Total Ocean Alkalinity (Pg C)	39 495	15.3	17.9	32.4	53.4	72.0	130
Total Ocean Carbon (Pg C)	37 321	584	587	600	619	634	681
Total Atmospheric Carbon (Pg C)	602	219	218	215	210	206	195
Sea Surface Calcite Saturation State	4.81	−0.841	−0.835	−0.813	−0.782	−0.755	−0.684
Sea Surface pH	8.16	−0.119	−0.119	−0.117	−0.114	−0.111	−0.104

BGD
8, 11863–11897, 2011

Table 4. Summary of the change in rain ratio and sediment output for years 1800–3500 for Suite S simulations. Values in column $S0_{1800}$ represent absolute output in the base model in year 1800. Subsequent columns show differences from 1800 to 3500 for each calcification sensitivity (S0 to S5).

	$S0_{1800}$	$S0_{3500-1800}$	$S1_{3500-1800}$	$S2_{3500-1800}$	$S3_{3500-1800}$	$S4_{3500-1800}$	$S5_{3500-1800}$
Rain Ratio Reaching Sediments (PIC : POC)	1.25	0.219	0.212	0.201	0.145	0.120	0.0699
Total Sediment Pore Layer $CaCO_3$ (Pg C)	1095	−32.0	−32.4	−36.5	−44.9	−51.6	−65.7
Additional $CaCO_3$ Buried in Sediments (Pg C)		11.4	7.4	−3.6	−13.6	−19.6	−22.6

BGD
8, 11863–11897, 2011

Table 5. Summary of the change in rain ratio and sediment output for years 1800–3500 for Suite M simulations. Values in column $M0_{1800}$ represent absolute output in the base model in year 1800. Subsequent columns show differences from 1800 to 3500 for each calcification sensitivity (M0 to M5).

	$M0_{1800}$	$M0_{3500-1800}$	$M1_{3500-1800}$	$M2_{3500-1800}$	$M3_{3500-1800}$	$M4_{3500-1800}$	$M5_{3500-1800}$
Rain Ratio Reaching Sediments (PIC : POC)	1.25	0.0996	0.0973	0.0863	0.0713	0.0592	0.0342
Total Sediment Pore Layer $CaCO_3$ (Pg C)	1095	−20.8	−18.4	−19.6	−21.0	−21.5	−21.8
Additional $CaCO_3$ Buried in Sediments (Pg C)		12.4	10.4	12.4	17.4	23.4	45.4

BGD
8, 11863–11897, 2011

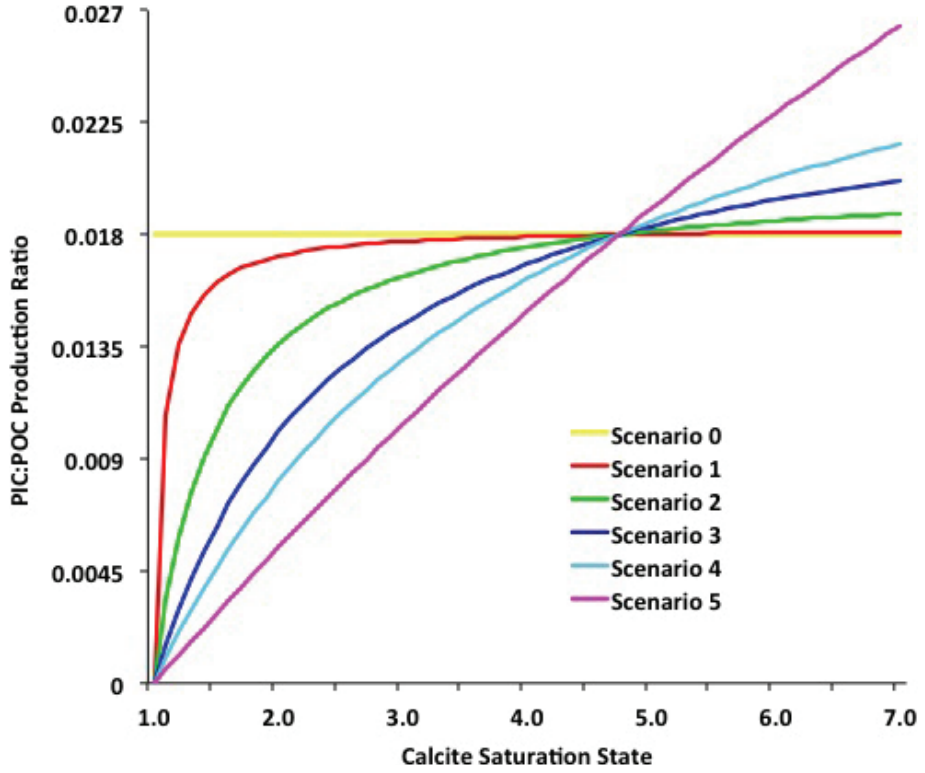

Fig. 1. $CaCO_3$: Particulate organic carbon production ratio dependence on calcite saturation state.

BGD
8, 11863–11897, 2011

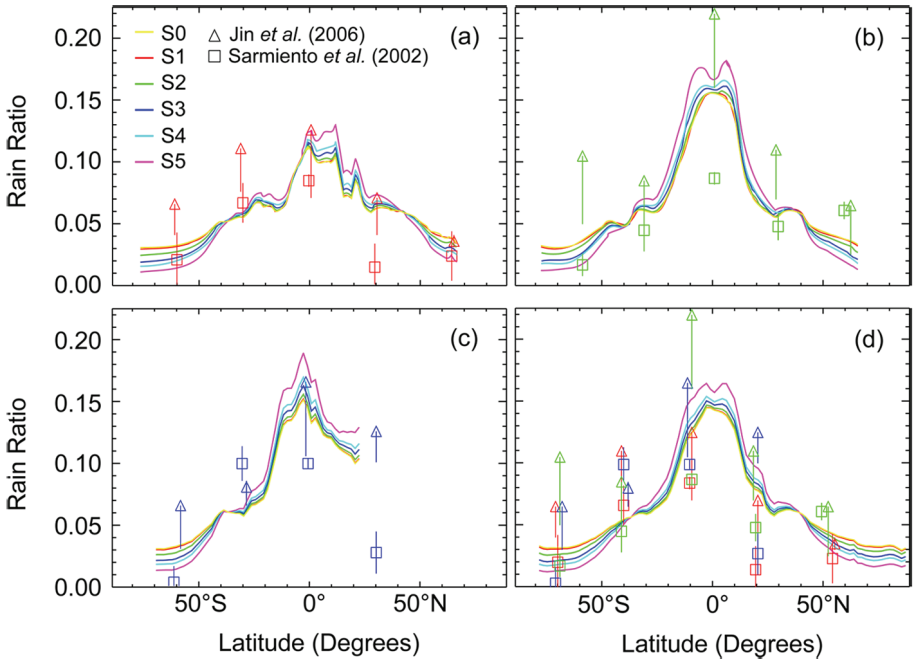

Fig. 2. Zonally averaged $CaCO_3$: Particulate organic carbon flux (rain ratio) across 130-m depth in comparison with observational estimates from Sarmiento et al. (2002) (square symbols) and Jin et al. (2006) (triangles) including their reported error bars (vertical lines) for the **(a)** Atlantic, **(b)** Pacific, and **(c)** Indian Oceans as well as **(d)** the global model mean.

BGD
8, 11863–11897, 2011

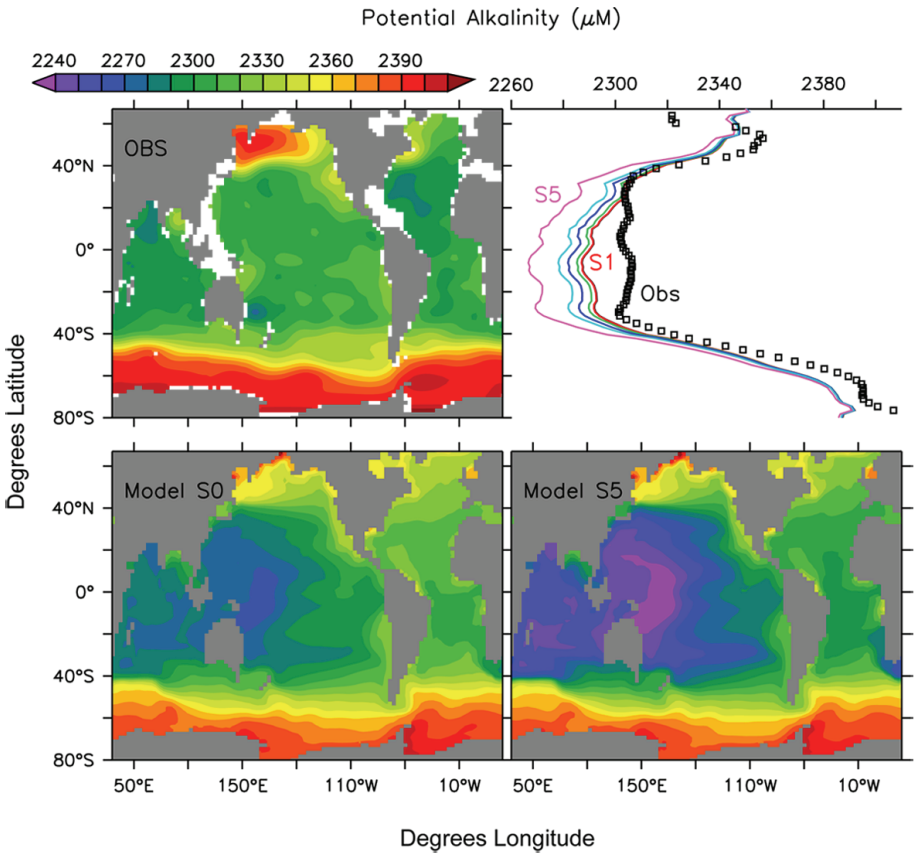

Fig. 3. Comparison of observed (top left) and modeled (bottom) surface distributions of potential alkalinity. The top right panel shows zonally averaged values for the observations (squares) and the different models (color lines). Note that the black line representing model S0 is overlain by the red line representing model S1 because both are almost undistinguishable.

BGD
8, 11863–11897, 2011

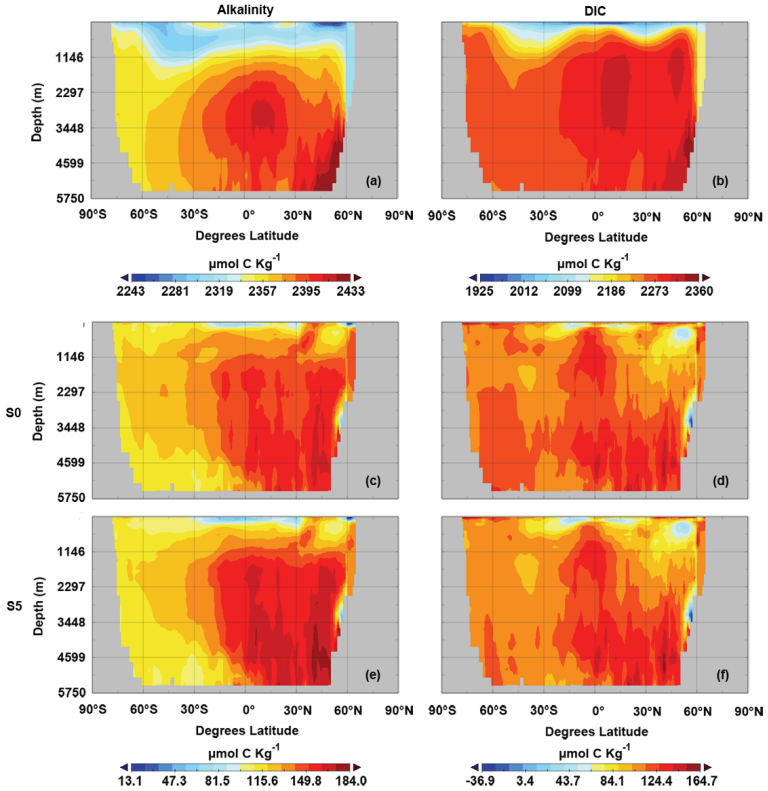

Fig. 4. Observed **(a)** ocean alkalinity and **(b)** dissolved inorganic carbon (Key et al., 2004). Panels (**c** and **e**) are plots of the difference between the zonally averaged global ocean alkalinity model output in year 1995 and observations for runs S0 and S5, respectively. Panels (**d** and **f**) are plots of the difference between the zonally averaged global dissolved inorganic carbon model output in year 1995 and observations for runs S0 and S5, respectively.

BGD
8, 11863–11897, 2011

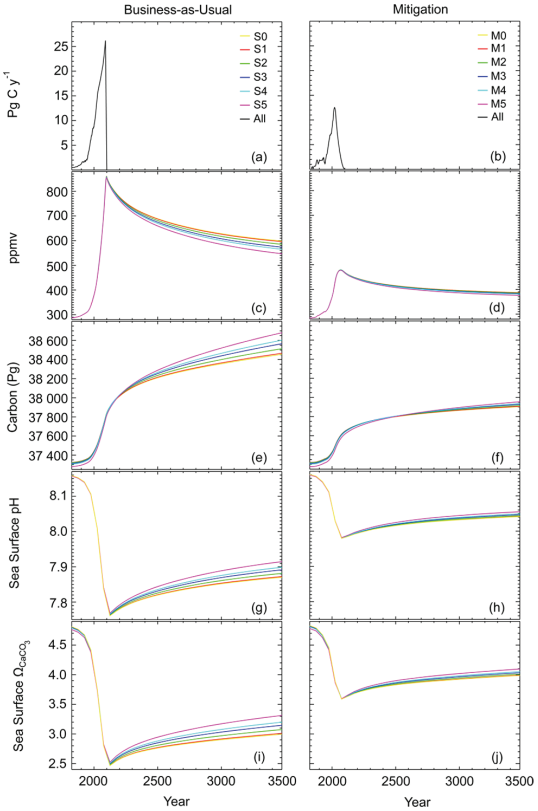

Fig. 5. (**a** and **b**) Change in anthropogenic CO_2 emissions, (**c** and **d**) globally averaged atmospheric CO_2 concentration, (**e** and **f**) globally averaged ocean carbon, (**g** and **h**) globally averaged sea surface pH, and (**i** and **j**) globally averaged calcite saturation state under a "business-as-usual" (Suite S) and a "mitigation" CO_2 emissions scenario (Suite M), respectively.

BGD
8, 11863–11897, 2011

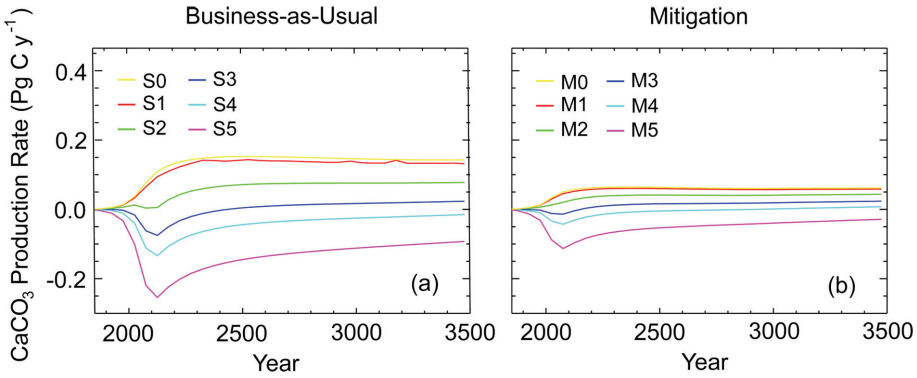

Fig. 6. Change in total sea surface $CaCO_3$ production rate under **(a)** a "business-as-usual" CO_2 emissions scenario (Suite S) and **(b)** under "mitigation" CO_2 emissions scenario (Suite M).

BGD
8, 11863–11897, 2011

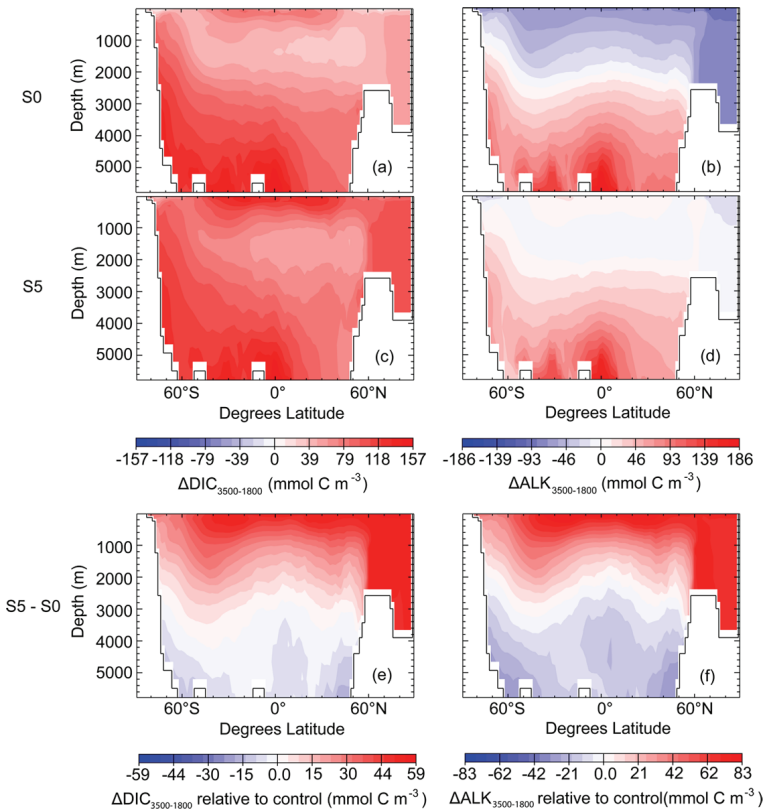

Fig. 7. **(a)** Global zonally averaged $\Delta DIC_{3500-1800}$ for run S0, **(b)** the global zonally averaged $\Delta ALK_{3500-1800}$ for runs S0, **(c)** the global zonally averaged $\Delta DIC_{3500-1800}$ for run S5, **(d)** the global zonally averaged $\Delta ALK_{3500-1800}$ for runs S5, **(e)** the difference in global zonally averaged $\Delta DIC_{3500-1800}$ relative to control (S0) for run S5, and **(f)** the difference in global zonally averaged $\Delta ALK_{3500-1800}$ relative to control (S0) for run S5.

BGD
8, 11863–11897, 2011

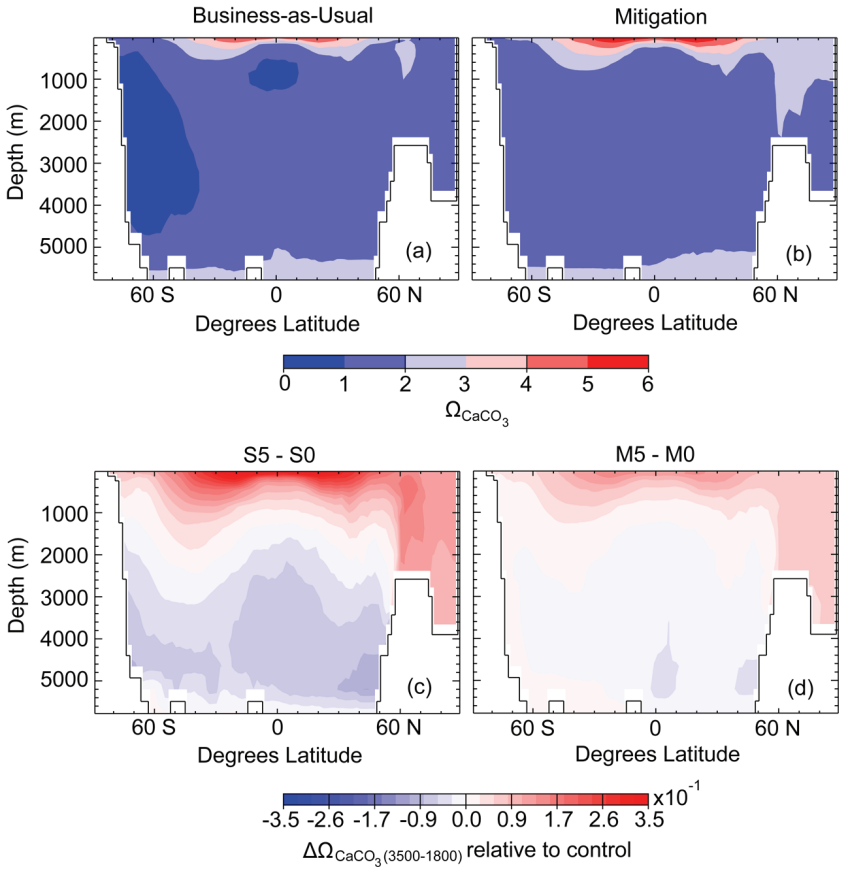

Fig. 8. Global zonally averaged ocean calcite saturation state in year 3500 for **(a)** run S0 and **(b)** run M0 and the global zonally averaged change in $\Delta\Omega_{CaCO_3(3500-1800)}$ relative to control (scenario 0) for **(c)** run S5 and **(d)** run M5, respectively.

BGD
8, 11863–11897, 2011

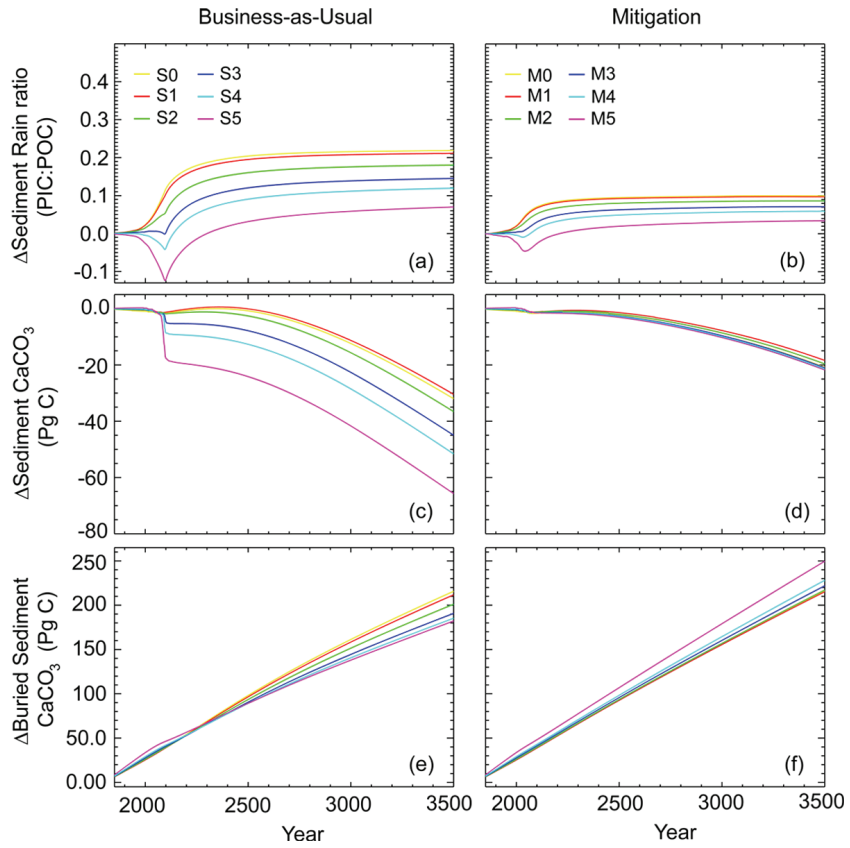

Fig. 9. (**a** and **b**) Change in globally averaged sediment rain ratio, (**c** and **d**) the total $CaCO_3$-carbon in the sediment surface pore layer, (**e** and **f**) and the total $CaCO_3$ buried in deeper marine sediments under a "business-as-usual" a "mitigation" CO_2 emissions scenario, respectively.

BGD
8, 11863–11897, 2011